UC Berkeley
UC Berkeley Previously Published Works

Title

Changes to the Chemical Composition of Soot from Heterogeneous Oxidation Reactions

Permalink

https://escholarship.org/uc/item/4bg264xf

Journal

The Journal of Physical Chemistry A, 119(7)

ISSN

1089-5639

Authors

Browne, Eleanor C
Franklin, Jonathan P
Canagaratna, Manjula R
et al.

Publication Date

2015-02-19

DOI

10.1021/jp511507d

Peer reviewed

Changes to the chemical composition of soot from heterogeneous oxidation reactions

Eleanor C. Browne[†], **Jonathan P. Franklin**[†], **Manjula R. Canagaratna**[‡], **Paola Massoli**[‡], **Thomas W. Kirchstetter**[§, ‖], **Douglas R. Worsnop**[‡], **Kevin R. Wilson**[⊥], and **Jesse H. Kroll**[†]

[†]Department of Civil and Environmental Engineering, Massachusetts Institute of Technology, Cambridge, Massachusetts, 02139, United States

[‡]Center for Aerosol and Cloud Chemistry, Aerodyne Research Inc., Billerica, Massachusetts, 01821, United States

[§]Environmental Energy and Technologies Division, Lawrence Berkeley National Laboratory, Berkeley, California, 94720, United States

[‖]Department of Civil and Environmental Engineering, University of California Berkeley, Berkeley, California, 94720, United States

[⊥]Chemical Sciences Division, Lawrence Berkeley National Laboratory, Berkeley, California, 94720, United States

Abstract

The atmospheric aging of soot particles, in which various atmospheric processes alter the particles' chemical and physical properties, is poorly understood and consequently is not well-represented in models. In this work, soot aging via heterogeneous oxidation by OH and ozone is investigated using an aerosol flow reactor coupled to a new high-resolution aerosol mass spectrometric technique that utilizes infrared vaporization and single-photon vacuum ultraviolet ionization. This analytical technique simultaneously measures the elemental and organic carbon components of soot, allowing for the composition of both fractions to be monitored. At oxidant exposures relevant to the particles' atmospheric lifetimes (the equivalent of several days of oxidation), the elemental carbon portion of the soot, which makes up the majority of the particle mass, undergoes no discernible changes in mass or composition. In contrast, the organic carbon (which in the case of methane flame soot is dominated by aliphatic species) is highly reactive, undergoing first the addition of oxygen-containing functional groups and ultimately the loss of organic carbon mass from fragmentation reactions that form volatile products. These changes occur on timescales comparable to other non-oxidative aging processes such as condensation, suggesting that further research into the combined effects of heterogeneous and condensational aging is needed to improve our ability to accurately predict the climate and health impacts of soot particles.

Graphical abstract
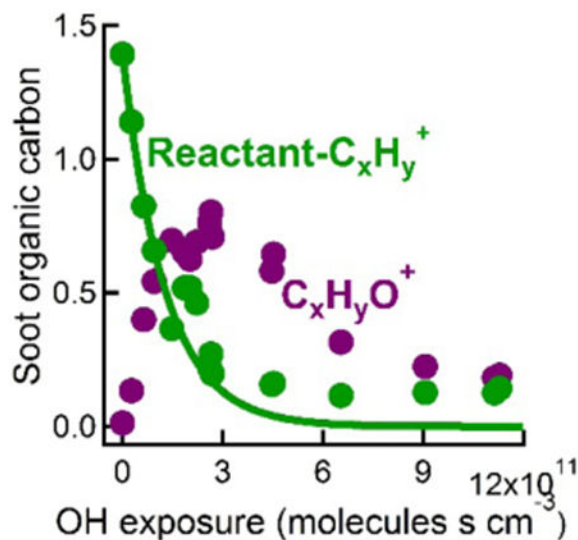
Introduction

Particulate and gaseous emissions from the incomplete combustion of fossil fuels, biofuels, and biomass are known to have important influences on both climate and human health.[1,2] An important component of such emissions are strongly light-absorbing carbonaceous particles ("soot"), which have recently received substantial attention due to their uncertain and potentially large climate impact.[3–6] Soot particles, containing a mixture of graphitic sp^2-bonded carbon (elemental carbon) and other co-emitted and internally mixed particulate organic and inorganic species, can have a dramatic influence on climate due to their strong absorption of light in the visible and ultraviolet regions of the electromagnetic spectrum. By some estimates, the climate warming by soot particles is second only to CO_2;[4] however, this is highly uncertain, with estimates for direct radiative forcing ranging from 0.17 W m^{-2} to 0.9 W m^{-2}.[3,4,6–9]

This wide range in estimated climate impacts is partly due to uncertainties associated with the atmospheric lifetime of soot.[4–6,9]. Soot lifetime is governed primarily by its wet deposition rate[8,10] and is thus determined by the particle surface's affinity for water (hydrophilicity). Since soot particles from many sources (e.g., fossil fuel combustion) tend to be initially hydrophobic when emitted,[4] atmospheric "aging" processes that increase the water-uptake properties of soot particles can play a major role in determining their atmospheric lifetimes. The parameter typically used to model such processes is the hydrophobic-to-hydrophilic conversion rate (hereinafter referred to as "conversion rate") of soot, which has been shown to have a controlling influence on the lifetimes and hence atmospheric burdens of soot particles. For example, in a sensitivity study by Koch et al.,[5] increasing the conversion rate by a factor of two resulted in a 19% decrease in modeled soot burden, while a rate a factor of two slower increased the modeled burden by 42%, thus indicating the importance of this conversion rate to the loading, and ultimately the overall climate impact, of soot particles.

The chemical and physical processes responsible for the conversion of soot from hydrophobic to hydrophilic include coagulation with other particles, condensation of gas-phase organic and inorganic species, and heterogeneous oxidation of the particle surface. Partly due to a lack of comprehensive and systematic laboratory studies on the rates of these chemical processes, global models have typically used conversion rates tuned to make modeled and measured soot concentrations match.[11,12] Traditionally, many global models have used fixed values for this rate;[5] however, as ambient observations increase in number, it has become apparent that a fixed value is insufficient to capture the seasonal, regional, and vertical variability of soot concentrations.[9,13–15] Consequently, more recent models have included improved treatments of conversion rates by explicitly modeling the coating of soot by secondary compounds, namely H_2SO_4,[9,14,16,17] or by parameterizing different aging processes for fossil-fuel and biomass-burning soot.[9] Although these more detailed treatments of the conversion rate typically perform better than fixed-rate assumptions,[9,14,16,17] measurement-model disagreements persist, indicating a specific need for a more thorough understanding of the processes that govern the water-uptake properties of soot particles.

Aging via heterogeneous oxidation of soot surfaces by gas-phase oxidants is one of the more uncertain soot aging processes. Most previous laboratory work on heterogeneous soot oxidation has focused on oxidation by ozone only. These studies have examined the kinetics of ozone uptake,[18–24] the rates of degradation and product formation of polycyclic aromatic hydrocarbons (PAHs, components of the soot organic carbon known to have carcinogenic and mutagenic effects),[25–28] and the changes to the particles' water uptake properties.[29–32] The heterogeneous oxidation of soot by the hydroxyl radical (OH) has received far less attention.[24,33–36] To our knowledge, the chemical changes to the soot surface have not been previously examined, although one study[33] has found an increase in the water uptake of oxidized soot relative to the unoxidized soot. Overall, there exists little information on the kinetics and the condensed-phase products of the reaction of OH with soot particles, limiting our ability to assess the role of heterogeneous oxidation in soot aging. In order to improve our understanding of this aging process, here we characterize the chemical changes that the organic and elemental carbon fractions of soot undergo upon heterogeneous oxidation by OH and ozone, using an aerosol flow reactor to oxidize the soot particles and a novel aerosol mass spectrometric technique to monitor their composition.

Experimental Section

VUV-SP-AMS

In this paper, soot chemical composition is characterized using a new technique for the measurement of both the organic and the elemental carbon fractions of the particles, involving a modified version of the Aerodyne soot particle aerosol mass spectrometer (SP-AMS).[37] The SP-AMS is a high-resolution time-of-flight aerosol mass spectrometer[38,39] that uses a 1064 nm YAG laser to vaporize refractory elemental carbon and non-refractory species associated with the elemental carbon. In the standard SP-AMS configuration, ionization of the vapor is achieved using electron impact (70 eV); in these experiments we instead use vacuum ultraviolet (VUV) single-photon ionization, utilizing VUV light from

the Chemical Dynamics Beamline (9.0.2) of the Advanced Light Source (ALS) at Lawrence Berkeley National Laboratory. This specific configuration is described in detail elsewhere.[40] Briefly, this combination of IR vaporization and VUV ionization requires that three beams – the laser, VUV light, and particle beam – all intersect within the ionization region of the mass spectrometer. The laser enters the ionization region perpendicular to the particle beam while the VUV enters from the back of the ionizer cage via a custom back flange 20° off center. This configuration necessitates the use of the large ionizer cage and removal of the thermal vaporizer.

Using VUV-SP-AMS allows for the sensitive monitoring of the chemical changes to organic compounds within the soot, which (as shown below) are far less abundant yet more reactive than the elemental carbon cores. Since ionization cross sections increase with increasing photon energy, this technique has a higher sensitivity to the organic carbon (ionization energies of ~7.4-11 eV[41]), than to the elemental carbon (ionization energy 11.6 eV for C_3,[42] the most abundant carbon cluster formed in the vaporization of elemental carbon). While tunable VUV radiation is available at the ALS, the present results focus on ionization at 12 eV only, allowing for the simultaneous measurement of the elemental and organic carbon while maintaining the enhanced sensitivity to organic species. Elemental and organic carbon are determined from their exact masses and ion formulae using high-resolution analysis of the low-mass ions ($m/z < 130$); due to the presence of numerous possible isobars at higher m/z (particularly at high oxidant exposures), the treatment of the mass spectrum at high m/z is mostly restricted to unit mass resolution. This choice does not affect the interpretation of the results because ions with $m/z < 130$ represent the majority of the signal for both the elemental and organic carbon (discussed in further detail in the Results section).

Flow tube set-up

Aging experiments were carried out in an oxidation flow reactor, previously developed for studies of the heterogeneous oxidation of organic particles;[43–45] the primary modification for the present study was the method of particle introduction, involving aerosolization of a suspension of flame soot in water. Flame soot generated from the fuel-rich combustion of methane in an inverted co-flow diffusion flame [46] was collected on filter paper and extracted with water using sonication. The resulting suspension underwent continuous sonication as it was atomized with a constant-output atomizer (TSI) using N_2 gas; particles were then passed through a diffusion dryer, and combined with the carrier flow (0.57 SLM of 17% O_2 in N_2 at ~30% RH). This flow was combined with 0.05 SLM flow of ozone in N_2/O_2 and 0.025 SLM of a hexane mixture (~5 ppm in N_2) to result in a total flow of 1 SLM through the flow tube. OH radicals were generated within the reactor via the 254 nm photolysis of ozone and subsequent reaction of O(^{1}D) with water. Exposure to the 254 nm radiation only (with no ozone addition) resulted in no measurable changes to the soot particles. Different OH exposures were achieved by modifying the ozone concentration in the flow tube; residence time in the flow tube remained constant at ~37 s. Ozone only (lights off) experiments were also done using similar concentrations of ozone as used in the OH experiments. The OH exposure was quantified by measuring the decay of hexane (initial mixing ratio of ~125 ppbv) using gas chromatography with flame ionization detection (GC-FID). GC-FID measurements are available for about half the experiment; OH exposure for the remainder of

the experiment was estimated using a regression derived from measured hexane and ozone concentrations from an experiment performed the same day over a similar ozone concentration range. Particles exiting the flow tube were sent to a scanning mobility particle sizer (TSI model 3080), for quantification of particle number and electrical mobility diameter, and to the VUV-SP-AMS, for measurements of chemical composition. Averaged over the course of the experiment, the SMPS-derived surface-area weighted geometric mean diameter of the soot was 155 nm, with a volume loading of 1.55×10^8 $\mu m^3/m^3$.

Results and Discussion

Composition of unoxidized soot

The unoxidized mass spectrum of the flame soot is shown in Fig. 1. For the purposes of this study, the elemental carbon core of the soot is determined from the sum of the high resolution ion intensities of the elemental carbon ions (formula C_x^+, where x is an integer from one to ten). Higher-mass C_x^+ ions are present in low abundances, with the total signal from the $C_{11 \ x \ 25}^+$ ions accounting for only 7% of the total $C_{x \ 10}^+$ signal. This represents an upper limit, due to the increasing likelihood of isobaric organic ions that are difficult to resolve at these high masses. The most abundant elemental carbon ion is C_3^+, accounting for $55.3 \pm 0.6\%$ (mean $\pm 1\sigma$) of the signal. The high abundance of C_3^+ is consistent with previous studies at 70 eV.[37,47,48] C_1^+ accounts for $10.2 \pm 0.6\%$ of the signal, C_2^+ is $11.8 \pm 0.3\%$, C_4^+ is $8.0 \pm 0.2\%$, and C_{5-10}^+ is $14.7 \pm 0.5\%$ of the signal. Since this C_x^+ fragmentation pattern was obtained via ionization at 12 eV, it is not directly comparable to the C_x^+ fragmentation pattern obtained when using electron impact ionization at 70 eV; these differences are explained in detail in a separate study.[40]

For unoxidized soot (Fig. 1a) the total intensity of the organic ions is similar to that of the C_x^+ ions, with the organic ions accounting for 62% of the $m/z < 130$ signal. Due to the higher sensitivity of VUV-SP-AMS to the organic carbon compared to the elemental carbon, these similar intensities do not imply similar abundances. In fact, as discussed in detail below, the organic carbon accounts for a small fraction of the soot mass (on the order of a few percent), consistent with previous measurements from this flame source.[46]

The organic carbon spectrum of unoxidized soot, shown in greater detail in Fig. 1b, is predominantly composed of low-mass fragments, with high-mass ions (m/z 130) representing only 30% of the organic signal. Based on high-resolution analysis, the organic fraction is dominated by reduced aliphatic hydrocarbons; ions typical of aromatic species (which typically have formulae of $C_nH_{0.5n}^+$ to $C_nH_n^+$ or $C_6H_5(CH_2)_n^+$)[49] account for <1% of the low m/z organic signal and oxygenated ions account for 5%. (Fig. 1b). Since VUV ionization efficiency is highly sensitive to the class of chemical compound (alkane, aromatic, etc.),[50] these contributions are not strictly equivalent to mass fractions within the particles. However, VUV ionization cross-sections of aromatics are generally larger than those of aliphatic species[50], implying that the organic species are predominately aliphatic in nature.

The total organic signal is primarily made up of ions of the form $C_nH_{2n+1}^+$ (32% of the $C_xH_y^+$ ions) and $C_nH_{2n-1}^+$ (35%). Other important ion series include $C_nH_{2n}^+$ and $C_nH_{2n-2}^+$, which account for 19% and 10%, respectively, of the $C_xH_y^+$ signal. These less-hydrogenated

ions are typical for fragments of aliphatic unsaturated hydrocarbons (with double bonds or rings). The ions at higher masses (identified using unit mass resolution) exhibit the same characteristic groupings spaced by 14 units out to about m/z 200. At higher masses ($m/z >$ 200), specific high molecular-weight ions become prevalent. These include m/z 202 and 216; high resolution analysis indicates that at least part of these signals are due to the ions $C_{16}H_{10}^+$ (Fig. S1) and $C_{17}H_{12}^+$ (Fig. S2), which correspond to polycyclic aromatic hydrocarbons (PAHs). An aliphatic ion at m/z 280 ($C_{20}H_{40}^+$) is also prominent (Fig. S3). The ion signal at m/z 252 (Fig. S4) includes contributions from both $C_{20}H_{12}^+$ (corresponding to a PAH) and the $C_{18}H_{36}^+$ (an aliphatic ion).

The continuous sonication of the soot, necessary to ensure a steady atomizer output and to prevent the atomizer from clogging, may result in changes to the soot composition.[51] To investigate this, we analyzed an unoxidized mass spectrum at the beginning of the experiment and a second unoxidized spectrum obtained about halfway through the experiment. These two mass spectra, both normalized to the C_x^+ signal, exhibit small changes in ion intensities. Compared to the first mass spectrum, the second shows a slight increase in oxygenated ions (up from 5% to 6% of the signal for $m/z < 130$) and in low-mass hydrocarbon ions (e.g., $C_4H_9^+$ increases by 14%), whereas it shows a decrease in the high-mass hydrocarbon ions (e.g., m/z 280 – primarily $C_{20}H_{40}^+$ – decreases by 13%). The PAH signals at m/z 202 and 216 show a disproportionately larger decrease than the aliphatic ions (m/z 202 decreases by 19%). Due to uncertainties regarding the effect of sonication on the PAHs over the course of the oxidation experiment, we do not attempt to quantify the oxidation of the PAHs.

The changes to the aliphatic ions resulting from sonication are smaller than the change observed from the lowest non-zero OH exposure (discussed in detail below), and thus sonication has a negligible impact on the interpretation of the OH oxidation of the aliphatic organic species. The changes observed during the ozone oxidation experiments (described below), which are more subtle, are comparable to the overall changes resulting from sonication; however, assuming that the changes arising from sonication occur linearly with time, the effects of sonication is expected to be small over the limited duration (~30 min) of the ozone experiment. Thus, the changes to soot particle composition as a result of sonication can be neglected when examining the chemical changes resulting from either OH or ozone oxidation.

Chemical changes resulting from OH oxidation

Over the range of oxidation conditions used here (maximum OH exposure equivalent to ~13 days of atmospheric exposure, assuming an atmospheric concentration of 10^6 molecules cm^{-3}), the mass spectrum of the elemental carbon (C_x^+) remains invariant. The C_x^+ signal also correlates well with the integrated volume from SMPS scans across all oxidation conditions ($R^2 = 0.91$) and the SMPS-derived average volume per particle shows no trend with OH exposure ($R^2 = 1 \times 10^{-5}$) despite large changes in the total organic signal (discussed below). This implies that the soot is primarily composed of elemental carbon (consistent with previous characterization of soot from this flame source)[46] and that the elemental fraction of the particles is inert to oxidation under atmospherically relevant oxidant

exposures. It also constrains the volume fraction of organic carbon in the soot to be similar to, or less than, the observed variation between subsequent SMPS measurements of integrated volume. This variation is, on average, 3% and results from both the stability of the atomizer and the reproducibility of SMPS scans.

In contrast to the elemental carbon fraction of the soot, the organic fraction undergoes dramatic changes upon oxidation; Figure 2 shows the evolving organic mass spectrum at various levels of OH exposure. All organic signals have been normalized to C_x^+ to account for atomizer output fluctuations. Since the changes resulting from ozone oxidation (discussed below) were much smaller than those observed for OH, no correction for oxidation by ozone is needed. OH oxidation increases the abundance of oxygenated ions ($C_xH_yO^+$ and $C_xH_yO_z^+$, where z>1) and decreases the total abundance of the ions containing only carbon and hydrogen ($C_xH_y^+$), consistent with previous AMS studies of the heterogeneous oxidation of organic aerosol.[45,52] Inspection of the $C_xH_y^+$ trend with oxidation indicates that while some of the ions continuously decrease with oxidation, others increase during the initial stages of oxidation. The $C_xH_y^+$ ions that decrease with oxidation follow the formula $C_nH_{2n+1}^+$ and $C_nH_{2n}^+$ with n=4-9, and $C_nH_{2n-1}^+$ and $C_nH_{2n-2}^+$ with n=6-9; we refer to these as "reactant-$C_xH_y^+$." The ions that increase with oxidation ("product-$C_xH_y^+$") follow the formula $C_nH_{2n+1}^+$ and $C_nH_{2n}^+$ (n=2-3), $C_nH_{2n-1}^+$ (n=2-5), $C_nH_{2n-2}^+$ (n=4-5), and $C_nH_{2n-3}^+$ (n=5-9). "Remainder-$C_xH_y^+$" contains all other ions with the formula $C_xH_y^+$. All the ions within this last group have a lower hydrogen-to-carbon ratio (H/C) than those in the reactant- or product-$C_xH_y^+$ groups, and either remain constant or increase with oxidation. While this is initially a small fraction of the total, its importance as a fraction of total $C_xH_y^+$ increases as oxidation proceeds and the total $C_xH_y^+$ intensity decreases.

At low oxidation levels, up to the equivalent of about two days of oxidation (assuming an average OH concentration of 10^6 molecules cm^{-3}), the total organic signal increases due to the increasing levels of the oxygenated ions. Since it is possible that the VUV ionization cross-sections are different for oxygenates than for the reduced hydrocarbons, this does not necessarily imply an increase in organic mass; however, it is clear that the oxygen content of the organic species increases with oxidation. This change is also reflected in the formulae of the product-$C_xH_y^+$ ions, which generally have a lower hydrogen content and/or smaller carbon numbers than the reactant-$C_xH_y^+$ ions. Although lower H/C values can indicate increasing levels of unsaturation, here they are likely to be fragments of the oxidized organic molecules that have undergone oxygen loss in the vaporization or ionization steps. This observation of increases in $C_xH_y^+$ ions with low H/C has also been observed by Kroll et al.[53] for the heterogeneous oxidation of diesel exhaust aerosol. The lower H/C and general increasing trend of the remainder-$C_xH_y^+$ ions suggests that these ions may also be the result of the fragmentation of oxygenates.

As the oxidant exposure increases, all ions attributed to oxygenates (including the product-$C_xH_y^+$) reach a maximum and then begin to decrease, with the $C_xH_yO_z^+$ signal peaking at noticeably higher OH exposures than either the product-$C_xH_y^+$ or the $C_xH_yO^+$ signal. This behavior is consistent with the evolution of multiple generations of oxidation products: early generations involve the addition of oxygen-containing functional groups, whereas later

generations are characterized by increased fragmentation that results in the loss of mass via the formation of small, volatile products.[45,54]

The effective rate of oxidation of the reduced organic molecules can be determined by fitting the decay in the reactant-$C_xH_y^+$ signal. The fit is restricted to include only the points at OH exposures of $< 9.5 \times 10^{10}$ molecules s cm^{-3}, for which measurements (rather than estimates) of OH exposure are available. This results in an effective second-order oxidation rate constant of the soot organic fraction by OH of $7.9 \pm 0.2 \times 10^{-12}$ cm^3 molecules^{-1} s^{-1}, equivalent to a lifetime of 1.5 days in the atmosphere (assuming a diurnally averaged OH of 10^6 molecules cm^{-3}). Since this rate is determined from the decay of many ions, it represents an average rate for the reaction of the various organic species, and is thus necessarily slower than the rate of the fastest-decaying ion. However, although all the reactant-$C_xH_y^+$ ions exhibit a decrease with increasing oxidant exposure, some of these ions may arise from fragmentation of high molecular weight oxygenates during vaporization or ionization. Inspection of various ions of relatively high abundance and high-resolution analysis of *m/z* 280 indicates that for individual high *m/z* ions the oxidation rate of may be up to a factor of two faster. We emphasize that this is an absolute upper limit and that the average rate for all the organics will be lower.

The $C_xH_y^+$ decay expected from this rate is shown extended out to higher oxidation levels in Fig. 3. For oxidant exposures up to $\sim 4 \times 10^{11}$ molecules s cm^{-3} (4.6 days), there is good agreement between the expected decay and the $C_xH_y^+$ measurement; however, at higher oxidation exposures the measured ion intensities begin to plateau at a non-zero value. This result may indicate that some fraction of the hydrocarbon is inaccessible to oxidation, possibly due to soot morphology. Often referred to as "shielding" of the organic species from oxidation, this phenomenon has previously been proposed to explain concentrations of soot-associated PAHs in remote regions that are inconsistent with laboratory measurements of PAH oxidative lifetimes.[55–57] Alternatively, this apparent plateau may be the result of the remaining organic species having a greatly reduced oxidation rate compared to those that reacted away initially.

The second-order rate constant can be used to calculate the initial uptake coefficient, γ_{OH}, defined here as the fraction of collisions of OH with soot particles that lead to reactive loss of reduced hydrocarbons:

$$\gamma = k_{reactant - CxHy + OH} \frac{4}{\bar{c}} OH S \quad (1)$$

Here k is the second-order reaction rate constant, $\bar{c}$ is the mean speed of the OH molecules (619 m s^{-1}), and S is total aerosol surface area per unit volume (cm^2/cm^3). Most treatments of the heterogeneous oxidation of organic aerosols assume the entire mass of the particle is reactive and thus the reactive organic mass is proportional to the particle volume.[43,44,53,58] Such an assumption is not valid in the present case, since most of the particle mass is non-reactive elemental carbon. Instead, the reactive organic carbon is present as a thin coating, and is therefore better described in terms of the particle surface area:

$$\text{reactan} - CxHy + = xS \quad (2)$$

where x is the surface area coverage of the organic molecules (molecules cm^{-2}). Substitution of Eq. 2 into Eq. 1 yields:

$$\gamma = 4kxc \quad (3)$$

Assuming a coating thickness of 1 nm and a density and molecular weight typical for a C_8 alkane/alkene (0.7 g cm^{-3} and 114 g mol^{-1}) results in a surface area coverage (x) of 3.7×10^{14} molecules cm^{-2} and an uptake coefficient (γ_{OH}) of 0.19. Due to uncertainties regarding the surface area coverage of organic species, which is complicated by the uncertain morphology and homogeneity of organic species distribution on a given soot particle, this number is not corrected for gas-phase diffusion; doing so would result in a 5% increase in the uptake coefficient. This calculation is also sensitive to the assumptions regarding coating thickness, density, and molecular weight. The coating thickness assumed above is consistent with the constraints on the organic volume fraction from the SMPS: a 1 nm coating thickness is equivalent to a volume fraction of 4%, assuming a spherical particle with a diameter of 155 nm (the surface-weighted mean diameter of the soot). Due to the large degree of organic fragmentation observed, it is difficult to constrain the density and molecular weight of the organic species. As an upper limit, we assume a C_{20} molecule (consistent with the peak observed at m/z 280) with a density of 0.8 g cm^{-3} and the same coating thickness. This results in a surface area coverage ($\times$) of 1.7×10^{14} molecules cm^{-2} and an uptake coefficient (γ) of 0.09.

The γ_{OH} derived here is broadly consistent to previous determinations for methane flame soot: Bertram et al.[24] report a range of 0.5 to 1 (average of 0.88) using a coated flow tube approach while Park et al.[34] report a larger range of 0.03 to 1 using a bead-filled flow tube. Differences between these values may be due to differences in the organic composition of the soot in the different experiments, though they also may arise from errors in the determination of surface characteristics (surface area or surface coverage) in the various experiments. The value of γ_{OH} derived here also agrees to within a factor of two of past measurements of γ_{OH} for squalane, a C_{30} branched alkane.[43]

Chemical changes resulting from ozone oxidation

Due to the short residence time in the flow tube (37 s) and the fact that ozone is present in the atmosphere at concentrations on the order of tens of ppbv, high ozone exposures (equivalent to several days in the atmosphere) could not be achieved. Instead, the maximum ozone exposure (3.1×10^{16} molecules s cm^{-3}) corresponds to about 9 h in the atmosphere (at 40 ppbv ozone), a much lower equivalent atmospheric exposure than in the OH experiments. The change in the various ion classes (using the same definitions as with the OH exposure) as a function of ozone oxidation is shown in Fig. 4. The changes observed with ozone were much smaller than those for OH; changes at the highest ozone concentration (the same

concentration used to achieve the highest OH exposure) were nearly equal in magnitude to those observed at the lowest non-zero OH exposure. This confirms the appropriateness of neglecting an ozone correction for the OH data presented above.

While the OH and ozone experiments differ in the magnitude of changes to ion intensities, the observed chemical changes to the soot in the two cases are similar; the reactant-$C_xH_y^+$ and product-$C_xH_y^+$ ions are the same as in the OH oxidation experiments and exhibit the same trends with increasing oxidation. Since ozone reacts with alkenes but not alkanes, this suggests the presence of alkenes. In addition to these two classes of ions, the $C_xH_yO^+$ ions also show a minor increase. The remaining classes of ions show no discernible trend.

Fitting an exponential decay (with no constraint on the zero oxidation value) to the reactant-$C_xH_y^+$ signal results in a second-order rate constant of $6 \pm 1 \times 10^{-18}$ cm^3 molecules^{-1} s^{-1}; including the zero-oxidation value in the fit increases the rate by 25%. This rate is equivalent to a lifetime of just under 2 days, assuming an ambient ozone concentration of 40 ppbv. This lifetime is comparable to that derived from the OH oxidation experiments, suggesting that the modest changes in the organic signal observed here are the result of low equivalent atmospheric exposures, and not from a lack of reactivity to ozone, and that the two oxidants are approximately equally efficient at oxidizing soot-associated organic species. The elemental carbon portion of soot is inert to oxidation by either oxidant.

The second-order rate, combined with the same set of assumptions as above for the aliphatic molecular weight, density, and surface coverage for a C_8 molecule results in a γ_{O_3} of 2×10^{-7}. This γ_{O_3} value is somewhat lower than those reported previously for oleic acid,[59] self-assembled alkene monolayers,[60,61] and soot,[18,19,23,62] which are typically on the order of 10^{-6} to 10^{-3}. Many of these studies, however, monitored only the ozone loss and the initial γ_{O_3} may be higher due to non-reactive ozone uptake on the surface; previous studies have reported that heterogeneous ozone loss occurs via a Langmuir-Hinshelwood mechanism, in which ozone first reversibly adsorbs to the surface before undergoing reaction.

Atmospheric implications and future work

This work shows that heterogeneous reactions with OH and ozone are efficient mechanisms for oxidizing aliphatic organic species present on soot particles. While the average timescales for such oxidation processes are on the order of 1-2 days, the detailed impact for a given particle will vary spatially and temporally due to variability in oxidant concentrations. For instance, the organic species on soot emitted in the late morning in a moderately polluted environment (with an OH concentration of 3×10^6 molecules cm^{-3} and 60 ppbv ozone) will have a lifetime of 8.5 hours, with the two oxidants contributing approximately equally to this reactivity. In contrast, soot emitted at night, when ozone concentrations are lower and oxidation by OH is negligible, will have a longer lifetime (> 30 h) with respect to oxidation. This lifetime is an upper limit given that the organic fraction of soot will also react with NO_3.[63]

These heterogeneous oxidation timescales can be compared to the timescales of other soot aging processes, which have been primarily determined from atmospheric observations of soot coating, and model estimates of the relative importance of condensation versus

coagulation. Particle-resolved models show diurnal trends in coating rates, with daytime aging resulting from condensation and occurring on the time scale of a few hours, and nighttime aging resulting mainly from coagulation and occurring on timescales closer to one day.[64–66] Atmospheric measurements indicate similar trends with daytime coating occurring on the timescale of hours[67–70] with faster coating timescales observed for soot from biomass burning and slower timescales for fossil fuel soot emissions.[69,71,72] At night the coating rate is slower,[70] consistent with the expected decrease in condensable gas production. Some atmospheric measurements, however, find that increasing plume age does not always result in increases in coating.[71] Although this may in part be due to preferential scavenging of coated soot,[71] it is also consistent with observations showing that biomass burning organic aerosol is semi-volatile and evaporates with aging[72–75]. Thus, the organic component of soot may remain exposed and subject to heterogeneous oxidation for extended periods of time.

These considerations suggest that heterogeneous oxidation of the organic fraction of soot occurs on timescales comparable to the coating timescales. It should be emphasized that the lifetime of the soot organic fraction is not necessarily equivalent to the lifetime for the hydrophobic-to-hydrophilic conversion of soot, particularly in cases where condensation and/or coagulation will render a fraction of the organic component of soot inaccessible to oxidation (although coating by organic species is also not necessarily equivalent to the hydrophobic-to-hydrophilic conversion rate). Nonetheless, heterogeneous oxidation will likely affect not only the primary soot organic fraction, but also condensed secondary organic species as well. In both cases, the heterogeneous oxidation of the organic fraction will alter how various gases (water, other inorganic and organic species) interact with the soot surface and thus will impact the overall soot aging.

The impact of heterogeneous oxidation on aging has been previously investigated using rates derived from the oxidation of PAHs by OH and ozone in a particle-resolved urban model[76] and in global models assuming oxidation by ozone only.[77–79] Such studies have generally found that although heterogeneous oxidation alone may result in the efficient oxidation of the surface PAHs,[76] it becomes less important when condensation and coagulation are included as aging processes.[77–79] To some extent, the reduced importance of heterogeneous oxidation as an aging mechanism in these studies results from the arbitrary reduction of the oxidation rate to some small fraction (often 1%) of its measured value, in order to account for "shielding" of the soot surface by condensed organic and inorganic species.[78,79] This scaling can have a dramatic effect on soot lifetimes: Croft et al.[78] found that changing this factor from 0.01 to 0.1 results in a decrease in the global mean lifetime of soot by almost 50% (from 9.5 days to 4.8 days) making it clear that better constraints on the relative roles of coating and heterogeneous oxidation are needed.

Overall, our results suggest that a more comprehensive treatment of heterogeneous oxidation of soot, including the oxidation of both aliphatics and aromatics by OH and ozone, is necessary to fully represent the aging process of soot. Due to variations in the abundance and composition of the organic carbon portion of soot,[48,80] as well as variations in the quantity and composition of co-emitted species, the relative rates of condensation and heterogeneous oxidation as aging processes will likely exhibit strong temporal and spatial variabilities. To fully constrain these processes, soot aging experiments in which

heterogeneous oxidation occurs in conjunction with the production of condensable gases (e.g., producing H_2SO_4 from the reaction of OH with SO_2 in the presence of soot) are needed. Conducting these experiments with a wider range of soot sources (which will vary in the organic composition) and including simultaneous measurements of the hygroscopicity and/or CCN activity of the soot as a function of OH exposure, coating material, and coating thickness will significantly improve the understanding of the aging, condensational lifetime, and ultimately the climate and health impacts of soot particles.

Acknowledgments

References

1. Crutzen PJ, Andreae MO. Biomass Burning in the Tropics: Impact on Atmospheric Chemistry and Biogeochemical Cycles. Science. 1990; 250:1669–1678. [PubMed: 17734705]

2. Grahame TJ, Klemm R, Schlesinger RB. Public Health and Components of Particulate Matter: The Changing Assessment of Black Carbon. J Air Waste Manage Assoc. 2014; 64:620–660.

3. Boucher, O., Randall, D., Artaxo, P., Bretherton, C., Feingold, G., Forster, P., Kerminen, VM., Kondo, Y., Liao, H., Lohmann, U., et al. Clouds and Aerosols. In: Stocker, TF.Qin, D.Tignor, M.Allen, SK.Boschung, J.Nauels, A.Xia, Y.Bex, V., Midgley, PM., editors. Climate Change 2013: The Physical Science Basis Contribution of Working Group I to the Fifth Assessment Report of the Intergovernmental Panel on Climate Change. Cambridge University Press; Cambridge, United Kingdom and New York, NY, USA:

4. Bond TC, Doherty SJ, Fahey DW, Forster PM, Berntsen T, DeAngelo BJ, Flanner MG, Ghan S, Kärcher B, Koch D, et al. Bounding the Role of Black Carbon in the Climate System: A Scientific Assessment. J Geophys Res Atmos. 2013; 118:5380–5552.

5. Koch D, Schulz M, Kinne S, McNaughton C, Spackman JR, Balkanski Y, Bauer S, Berntsen T, Bond TC, Boucher O, et al. Evaluation of Black Carbon Estimations in Global Aerosol Models. Atmos Chem Phys. 2009; 9:9001–9026.

6. Samset BH, Myhre G, Herber A, Kondo Y, Li SM, Moteki N, Koike M, Oshima N, Schwarz JP, Balkanski Y, et al. Modeled Black Carbon Radiative Forcing and Atmospheric Lifetime in AeroCom Phase II Constrained by Aircraft Observations. Atmos Chem Phys Discuss. 2014; 14:20083–20115.

7. Ramanathan V, Carmichael G. Global and Regional Climate Changes due to Black Carbon. Nature Geosci. 2008; 1:221–227.

8. Wang Q, Jacob DJ, Spackman JR, Perring AE, Schwarz JP, Moteki N, Marais EA, Ge C, Wang J, Barrett SRH. Global Budget and Radiative Forcing of Black Carbon Aerosol: Constraints from Pole-to-Pole (HIPPO) Observations across the Pacific. J Geophys Res Atmos. 2014; 119:195–206.

9. Wang X, Heald CL, Ridley DA, Schwarz JP, Spackman JR, Perring AE, Coe H, Liu D, Clarke AD. Exploiting Simultaneous Observational Constraints on Mass and Absorption to Estimate the Global Direct Radiative Forcing of Black Carbon and Brown Carbon. Atmos Chem Phys. 2014; 14:10989–11010.

10. Jacobson MZ. Short-Term Effects of Controlling Fossil-Fuel Soot, Biofuel Soot and Gases, and Methane on Climate, Arctic Ice, and Air Pollution Health. J Geophys Res. 2010; 115:D14209.

11. Cooke WF, Wilson JJN. A Global Black Carbon Aerosol Model. J Geophys Res. 1996; 101:19395–19409.

12. Park RJ, Jacob DJ, Palmer PI, Clarke AD, Weber RJ, Zondlo MA, Eisele FL, Bandy AR, Thornton DC, Sachse GW, et al. Export Efficiency of Black Carbon Aerosol in Continental Outflow: Global Implications. J Geophys Res. 2005; 110:D11205.

13. Schwarz JP, Spackman JR, Gao RS, Watts LA, Stier P, Schulz M, Davis SM, Wofsy SC, Fahey DW. Global-Scale Black Carbon Profiles Observed in the Remote Atmosphere and Compared to Models. Geophys Res Lett. 2010; 37:L18812.

14. Liu J, Fan S, Horowitz LW, Levy H. Evaluation of Factors Controlling Long-Range Transport of Black Carbon to the Arctic. J Geophys Res. 2011; 116:D04307.

15. Stier P, Feichter J, Kinne S, Kloster S, Vignati E, Wilson J, Ganzeveld L, Tegen I, Werner M, Balkanski Y, et al. The Aerosol-Climate Model ECHAM5-HAM. Atmos Chem Phys. 2005; 5:1125–1156.

16. Vignati E, Karl M, Krol M, Wilson J, Stier P, Cavalli F. Sources of Uncertainties in Modelling Black Carbon at the Global Scale. Atmos Chem Phys. 2010; 10:2595–2611.

17. Park SH, Gong SL, Bouchet VS, Gong W, Makar PA, Moran MD, Stroud CA, Zhang J. Effects of Black Carbon Aging on Air Quality Predictions and Direct Radiative Forcing Estimation. Tellus B. 2011; 63B:1026–1039.

18. Lelièvre S, Bedjanian Y, Pouvesle N, Delfau JL, Vovelle C, Le Bras G. Heterogeneous Reaction of Ozone with Hydrocarbon Flame Soot. Phys Chem Chem Phys. 2004; 6:1181–1191.

19. Kamm S, Möhler O, Naumann KH, Saathoff H, Schurath U. The Heterogeneous Reaction of Ozone with Soot Aerosol. Atmos Environ. 1999; 33:4651–4661.

20. Smith DM, Chughtai AR. Reaction Kinetics of Ozone at Low Concentrations with N-Hexane Soot. J Geophys Res. 1996; 101:19607–19620.

21. Disselkamp RS, Carpenter MA, Cowin JP, Berkowitz CM, Chapman EG, Zaveri RA, Laulainen NS. Ozone Loss in Soot Aerosols. J Geophys Res. 2000; 105:9767–9771.

22. Rogaski CA, Golden DM, Williams LR. Reactive Uptake and Hydration Experiments on Amorphous Carbon Treated with NO_2, SO_2, O_3, HNO_3, and H_2SO_4. Geophys Res Lett. 1997; 24:381–384.

23. McCabe J, Abbatt JPD. Heterogeneous Loss of Gas-Phase Ozone on n-Hexane Soot Surfaces: Similar Kinetics to Loss on Other Chemically Unsaturated Solid Surfaces†. J Phys Chem C. 2009; 113:2120–2127.

24. Bertram AK, Ivanov AV, Hunter M, Molina LT, Molina MJ. The Reaction Probability of OH on Organic Surfaces of Tropospheric Interest. J Phys Chem A. 2001; 105:9415–9421.

25. Kahan TF, Kwamena NOA, Donaldson DJ. Heterogeneous Ozonation Kinetics of Polycyclic Aromatic Hydrocarbons on Organic Films. Atmos Environ. 2006; 40:3448–3459.

26. Kwamena NOA, Earp ME, Young CJ, Abbatt JPD. Kinetic and Product Yield Study of the Heterogeneous Gas-Surface Reaction of Anthracene and Ozone. J Phys Chem A. 2006; 110:3638–3646. [PubMed: 16526646]

27. Pöschl U, Letzel T, Schauer C, Niessner R. Interaction of Ozone and Water Vapor with Spark Discharge Soot Aerosol Particles Coated with Benzo[a]pyrene: O_3 and H_2O Adsorption, Benzo[a]pyrene Degradation, and Atmospheric Implications. J Phys Chem A. 2001; 105:4029–4041.

28. Perraudin E, Budzinski H, Villenave E. Kinetic Study of the Reactions of Ozone with Polycyclic Aromatic Hydrocarbons Adsorbed on Atmospheric Model Particles. J Atmos Chem. 2007; 56:57–82.

29. Weingartner E, Burtscher H, Baltensperger U. Hygroscopic Properties of Carbon and Diesel Soot Particles. Atmos Environ. 1997; 31:2311–2327.

30. Liu Y, Liu C, Ma J, Ma Q, He H. Structural and Hygroscopic Changes of Soot during Heterogeneous Reaction with O_3. Phys Chem Chem Phys. 2010; 12:10896–10903. [PubMed: 20657898]

31. Chughtai AR, Jassim JA, Peterson JH, Stedman DH, Smith DM. Spectroscopic and Solubility Characteristics of Oxidized Soots. Aerosol Sci Technol. 1991; 15:112–126.

32. Decesari S, Facchini MC, Matta E, Mircea M, Fuzzi S, Chughtai AR, Smith DM. Water Soluble Organic Compounds Formed by Oxidation of Soot. Atmos Environ. 2002; 36:1827–1832.

33. Zuberi B, Johnson KS, Aleks GK, Molina LT, Molina MJ, Laskin A. Hydrophilic Properties of Aged Soot. Geophys Res Lett. 2005; 32:L01807.

34. Park JH, Ivanov AV, Molina MJ. Effect of Relative Humidity on OH Uptake by Surfaces of Atmospheric Importance. J Phys Chem A. 2008; 112:6968–6977. [PubMed: 18593137]

35. Vlasenko A, George IJ, Abbatt JPD. Formation of Volatile Organic Compounds in the Heterogeneous Oxidation of Condensed-Phase Organic Films by Gas-Phase OH. J Phys Chem A. 2008; 112:1552–1560. [PubMed: 18225872]

36. Bedjanian Y, Nguyen ML, Le Bras G. Kinetics of the Reactions of Soot Surface-Bound Polycyclic Aromatic Hydrocarbons with the OH Radicals. Atmos Environ. 2010; 44:1754–1760.

37. Onasch TB, Trimborn A, Fortner EC, Jayne JT, Kok GL, Williams LR, Davidovits P, Worsnop DR. Soot Particle Aerosol Mass Spectrometer: Development, Validation, and Initial Application. Aerosol Sci Technol. 2012; 46:804–817.

38. DeCarlo PF, Kimmel JR, Trimborn A, Northway MJ, Jayne JT, Aiken AC, Gonin M, Fuhrer K, Horvath T, Docherty KS, et al. Field-Deployable, High-Resolution, Time-of-Flight Aerosol Mass Spectrometer. Anal Chem. 2006; 78:8281–8289. [PubMed: 17165817]

39. Canagaratna MR, Jayne JT, Jimenez JL, Allan JD, Alfarra MR, Zhang Q, Onasch TB, Drewnick F, Coe H, Middlebrook A, et al. Chemical and Microphysical Characterization of Ambient Aerosols with the Aerodyne Aerosol Mass Spectrometer. Mass Spectrom Rev. 2007; 26:185–222. [PubMed: 17230437]

40. Canagaratna MR, Massoli P, Browne EC, Franklin JP, Wilson KR, Onasch TB, Kirchstetter TW, Fortner EC, Kolb CE, Jayne JT, et al. Chemical Compositions of Black Carbon Particle Cores and Coatings via Soot Particle Aerosol Mass Spectrometry with Photoionization and Electron Ionization. submitted to J Phys Chem A. 2014

41. Lias, SG. Ionization Energy Evaluation. In: Linstrom, PJ., Mallard, WG., editors. NIST Chemistry WebBook, NIST Standard Reference Database Number 69. National Institute of Standards and Technology; Gaithersburg MD: p. 20899

42. Belau L, Wheeler SE, Ticknor BW, Ahmed M, Leone SR, Allen WD, Schaefer HF, Duncan MA. Ionization Thresholds of Small Carbon Clusters: Tunable VUV Experiments and Theory. J Am Chem Soc. 2007; 129:10229–10243. [PubMed: 17655303]

43. Smith JD, Kroll JH, Cappa CD, Che DL, Liu CL, Ahmed M, Leone SR, Worsnop DR, Wilson KR. The Heterogeneous Reaction of Hydroxyl Radicals with Sub-Micron Squalane Particles: A Model System for Understanding the Oxidative Aging of Ambient Aerosols. Atmos Chem Phys. 2009; 9:3209–3222.

44. Kessler SH, Smith JD, Che DL, Worsnop DR, Wilson KR, Kroll JH. Chemical Sinks of Organic Aerosol: Kinetics and Products of the Heterogeneous Oxidation of Erythritol and Levoglucosan. Environ Sci Technol. 2010; 44:7005–7010. [PubMed: 20707414]

45. Kroll JH, Smith JD, Che DL, Kessler SH, Worsnop DR, Wilson KR. Measurement of Fragmentation and Functionalization Pathways in the Heterogeneous Oxidation of Oxidized Organic Aerosol. Phys Chem Chem Phys. 2009; 11:8005–8014. [PubMed: 19727507]

46. Kirchstetter TW, Novakov T. Controlled Generation of Black Carbon Particles from a Diffusion Flame and Applications in Evaluating Black Carbon Measurement Methods. Atmos Environ. 2007; 41:1874–1888.

47. Massoli P, Fortner EC, Canagaratna MR, Williams LR, Zhang Q, Sun Y, Schwab JJ, Trimborn A, Onasch TB, Demerjian KL, et al. Pollution Gradients and Chemical Characterization of Particulate Matter from Vehicular Traffic near Major Roadways: Results from the 2009 Queens College Air Quality Study in NYC. Aerosol Sci Technol. 2012; 46:1201–1218.

48. Corbin JC, Sierau B, Gysel M, Laborde M, Keller A, Kim J, Petzold A, Onasch TB, Lohmann U, Mensah AA. Mass Spectrometry of Refractory Black Carbon Particles from Six Sources: Carbon-Cluster and Oxygenated Ions. Atmos Chem Phys. 2014; 14:2591–2603.

49. McLafferty, FW., Ture ek, F. Interpretation of Mass Spectra. University Science Books; 1993.

50. Hanley L, Zimmermann R. Light and Molecular Ions: The Emergence of Vacuum UV Single-Photon Ionization in MS. Anal Chem. 2009; 81:4174–4182. [PubMed: 19476385]

51. Miljevic B, Hedayat F, Stevanovic S, Fairfull-Smith KE, Bottle SE, Ristovski ZD. To Sonicate or Not to Sonicate PM Filters: Reactive Oxygen Species Generation Upon Ultrasonic Irradiation. Aerosol Sci Technol. 2014; doi: 10.1080/02786826.2014.981330

52. George IJ, Vlasenko A, Slowik JG, Broekhuizen K, Abbatt JPD. Heterogeneous Oxidation of Saturated Organic Aerosols by Hydroxyl Radicals: Uptake Kinetics, Condensed-Phase Products, and Particle Size Change. Atmos Chem Phys. 2007; 7:4187–4201.

53. Kroll JH, Smith JD, Worsnop DR, Wilson KR. Characterisation of Lightly Oxidised Organic Aerosol Formed from the Photochemical Aging of Diesel Exhaust Particles. Environ Chem. 2012; 9:211–220.

54. Wilson KR, Smith JD, Kessler SH, Kroll JH. The Statistical Evolution of Multiple Generations of Oxidation Products in the Photochemical Aging of Chemically Reduced Organic Aerosol. Phys Chem Chem Phys. 2012; 14:1468–1479. [PubMed: 22158973]

55. Kwamena NOA, Staikova MG, Donaldson DJ, George IJ, Abbatt JPD. Role of the Aerosol Substrate in the Heterogeneous Ozonation Reactions of Surface-Bound PAHs. J Phys Chem A. 2007; 111:11050–11058. [PubMed: 17927163]

56. Friedman CL, Pierce JR, Selin NE. Assessing the Influence of Secondary Organic versus Primary Carbonaceous Aerosols on Long-Range Atmospheric Polycyclic Aromatic Hydrocarbon Transport. Environ Sci Technol. 2014; 48:3293–3302. [PubMed: 24564497]

57. Zhou S, Lee AKY, McWhinney RD, Abbatt JPD. Burial Effects of Organic Coatings on the Heterogeneous Reactivity of Particle-Borne Benzo[a]pyrene (BaP) toward Ozone. J Phys Chem A. 2012; 116:7050–7056. [PubMed: 22676584]

58. Robinson AL, Donahue NM, Rogge WF. Photochemical Oxidation and Changes in Molecular Composition of Organic Aerosol in the Regional Context. J Geophys Res. 2006; 111:D03302.

59. Sage AM, Weitkamp EA, Robinson AL, Donahue NM. Reactivity of Oleic Acid in Organic Particles: Changes in Oxidant Uptake and Reaction Stoichiometry with Particle Oxidation. Phys Chem Chem Phys. 2009; 11:7951–7962. [PubMed: 19727502]

60. Dubowski Y, Vieceli J, Tobias DJ, Gomez A, Lin A, Nizkorodov SA, McIntire TM, Finlayson-Pitts BJ. Interaction of Gas-Phase Ozone at 296 K with Unsaturated Self-Assembled Monolayers: A New Look at an Old System. J Phys Chem A. 2004; 108:10473–10485.

61. Moise T, Rudich Y. Reactive Uptake of Ozone by Proxies for Organic Aerosols: Surface versus Bulk Processes. J Geophys Res. 2000; 105:14667–14676.

62. Longfellow CA, Ravishankara AR, Hanson DR. Reactive and Nonreactive Uptake on Hydrocarbon Soot: HNO_3, O_3, and N_2O_5. J Geophys Res. 2000; 105:24345–24350.

63. Mak J, Gross S, Bertram AK. Uptake of NO_3 on Soot and Pyrene Surfaces. Geophys Res Lett. 2007; 34:L10804.

64. Riemer N, West M, Zaveri RA, Easter RC. Simulating the Evolution of Soot Mixing State with a Particle-Resolved Aerosol Model. J Geophys Res. 2009; 114:D09202.

65. Riemer N, West M, Zaveri R, Easter R. Estimating Black Carbon Aging Time-Scales with a Particle-Resolved Aerosol Model. J Aerosol Sci. 2010; 41:143–158.

66. Riemer N, Vogel H, Vogel B. Soot Aging Time Scales in Polluted Regions during Day and Night. Atmos Chem Phys. 2004; 4:1885–1893.

67. Moteki N, Kondo Y, Miyazaki Y, Takegawa N, Komazaki Y, Kurata G, Shirai T, Blake DR, Miyakawa T, Koike M. Evolution of Mixing State of Black Carbon Particles: Aircraft Measurements over the Western Pacific in March 2004. Geophys Res Lett. 2007; 34:L11803.

68. Moffet RC, Prather KA. In-Situ Measurements of the Mixing State and Optical Properties of Soot with Implications for Radiative Forcing Estimates. Proc Natl Acad Sci. 2009; 106:11872–11877. [PubMed: 19581581]

69. Schwarz JP, Gao RS, Spackman JR, Watts LA, Thomson DS, Fahey DW, Ryerson TB, Peischl J, Holloway JS, Trainer M, et al. Measurement of the Mixing State, Mass, and Optical Size of Individual Black Carbon Particles in Urban and Biomass Burning Emissions. Geophys Res Lett. 2008; 35:L13810.

70. Cheng YF, Su H, Rose D, Gunthe SS, Berghof M, Wehner B, Achtert P, Nowak A, Takegawa N, Kondo Y, et al. Size-Resolved Measurement of the Mixing State of Soot in the Megacity Beijing, China: Diurnal Cycle, Aging and Parameterization. Atmos Chem Phys. 2012; 12:4477–4491.

71. Subramanian R, Kok GL, Baumgardner D, Clarke A, Shinozuka Y, Campos TL, Heizer CG, Stephens BB, de Foy B, Voss PB, et al. Black Carbon over Mexico: The Effect of Atmospheric Transport on Mixing State, Mass Absorption Cross-Section, and BC/CO Ratios. Atmos Chem Phys. 2010; 10:219–237.

72. Akagi SK, Craven JS, Taylor JW, McMeeking GR, Yokelson RJ, Burling IR, Urbanski SP, Wold CE, Seinfeld JH, Coe H, et al. Evolution of Trace Gases and Particles Emitted by a Chaparral Fire in California. Atmos Chem Phys. 2012; 12:1397–1421.

73. Grieshop AP, Donahue NM, Robinson AL. Laboratory Investigation of Photochemical Oxidation of Organic Aerosol from Wood Fires 2: Analysis of Aerosol Mass Spectrometer Data. Atmos Chem Phys. 2009; 9:2227–2240.

74. Huffman JA, Docherty KS, Aiken AC, Cubison MJ, Ulbrich IM, DeCarlo PF, Sueper D, Jayne JT, Worsnop DR, Ziemann PJ, et al. Chemically-Resolved Aerosol Volatility Measurements from Two Megacity Field Studies. Atmos Chem Phys. 2009; 9:7161–7182.

75. Huffman JA, Docherty KS, Mohr C, Cubison MJ, Ulbrich IM, Ziemann PJ, Onasch TB, Jimenez JL. Chemically-Resolved Volatility Measurements of Organic Aerosol from Different Sources. Environ Sci Technol. 2009; 43:5351–5357. [PubMed: 19708365]

76. Kaiser JC, Riemer N, Knopf DA. Detailed Heterogeneous Oxidation of Soot Surfaces in a Particle-Resolved Aerosol Model. Atmos Chem Phys. 2011; 11:4505–4520.

77. Tsigaridis K, Kanakidou M. Global Modelling of Secondary Organic Aerosol in the Troposphere: A Sensitivity Analysis. Atmos Chem Phys. 2003; 3:1849–1869.

78. Croft B, Lohmann U, von Salzen K. Black Carbon Ageing in the Canadian Centre for Climate Modelling and Analysis Atmospheric General Circulation Model. Atmos Chem Phys. 2005; 5:1931–1949.

79. Huang Y, Wu S, Dubey MK, French NHF. Impact of Aging Mechanism on Model Simulated Carbonaceous Aerosols. Atmos Chem Phys. 2013; 13:6329–6343.

80. Slowik JG, Stainken K, Davidovits P, Williams LR, Jayne JT, Kolb CE, Worsnop DR, Rudich Y, DeCarlo PF, Jimenez JL. Particle Morphology and Density Characterization by Combined Mobility and Aerodynamic Diameter Measurements. Part 2: Application to Combustion-Generated Soot Aerosols as a Function of Fuel Equivalence Ratio. Aerosol Sci Technol. 2004; 38:1206–1222.
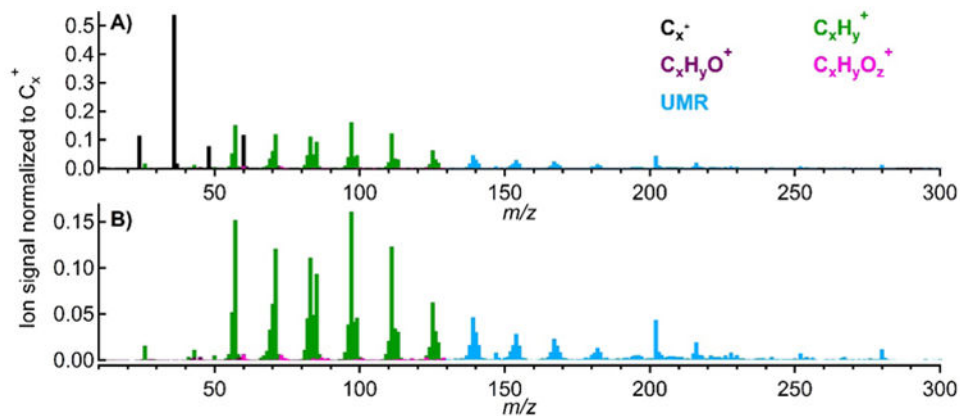
Figure 1.
Mass spectra for unoxidized flame soot (normalized to total C_x^+ signal). For clarity, reactant-, product-, and remainder-$C_xH_y^+$ are lumped together into $C_xH_y^+$. Panel (A): both C_x^+ and organic ions; panel (B): same as A, but showing the organic ions only. High-resolution analysis is shown only for $m/z < 130$; analysis for $m/z \geq 130$ is restricted to unit mass resolution (UMR). The elemental carbon (C_x^+) signal is dominated by C_{1-5}^+ ions. The organic mass spectrum indicates the predominance of reduced, aliphatic organic species.
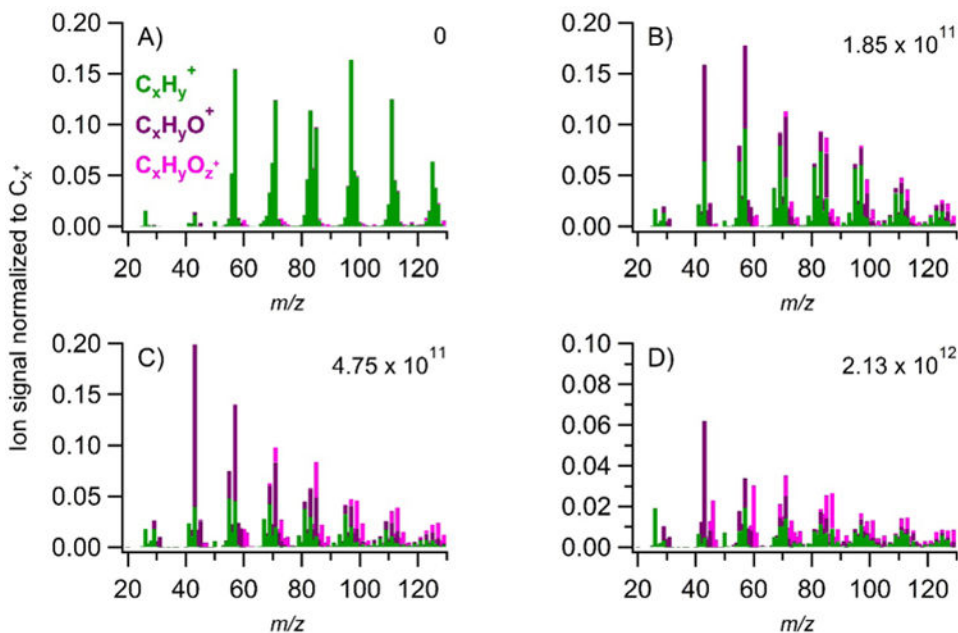
Figure 2.
Changes in the flame soot mass spectra with increasing OH exposure. OH exposure (in molecules s cm^{-3}) is noted in the upper right of each panel. For clarity reactant-, product-, and remainder-$C_xH_y^+$ are lumped together into $C_xH_y^+$. Increasing oxidation initially results in an increase in oxygenated ions. Reduced ions with higher H/C values decrease with increasing oxidation (reactant-$C_xH_y^+$) while those with lower H/C increase as oxidation increases (product-$C_xH_y^+$). At high levels of oxidation (panel D, which has a different y-axis range), all ions show a decrease in intensity.
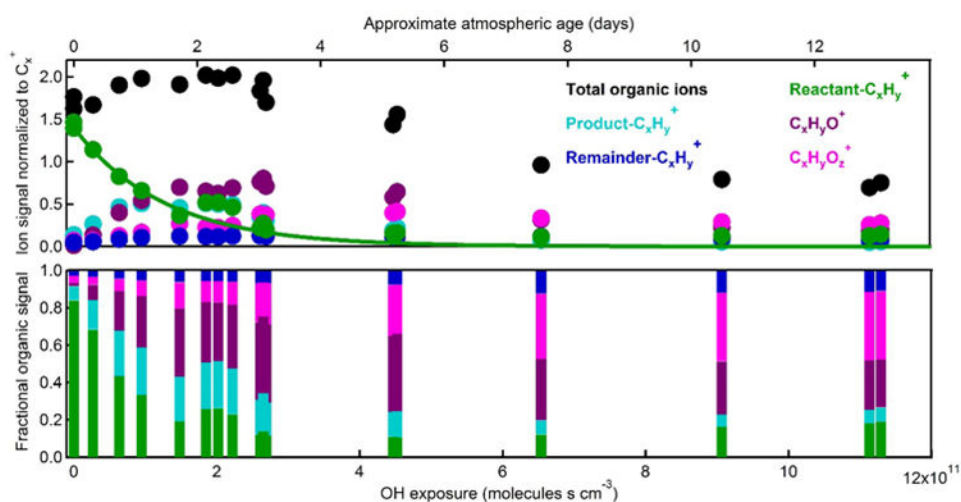
Figure 3.
Changes in ion signal for each class of ions as a function of OH exposure. The approximate atmospheric age assumes a 24-h average OH concentration of 10^6 molecules cm^{-3}. The OH exposures above 2.5×10^{11} molecules s cm^{-3} are estimated using the procedure described in the text. Top panel: ion classes normalized to total C_x^+. The rate of reactant-$C_xH_y^+$ decay is fit using data from the four lowest OH exposures. The solid green line shows the extrapolation of this fit to higher exposure levels. Bottom panel: fractional contribution of each ion class to the total organic signal.
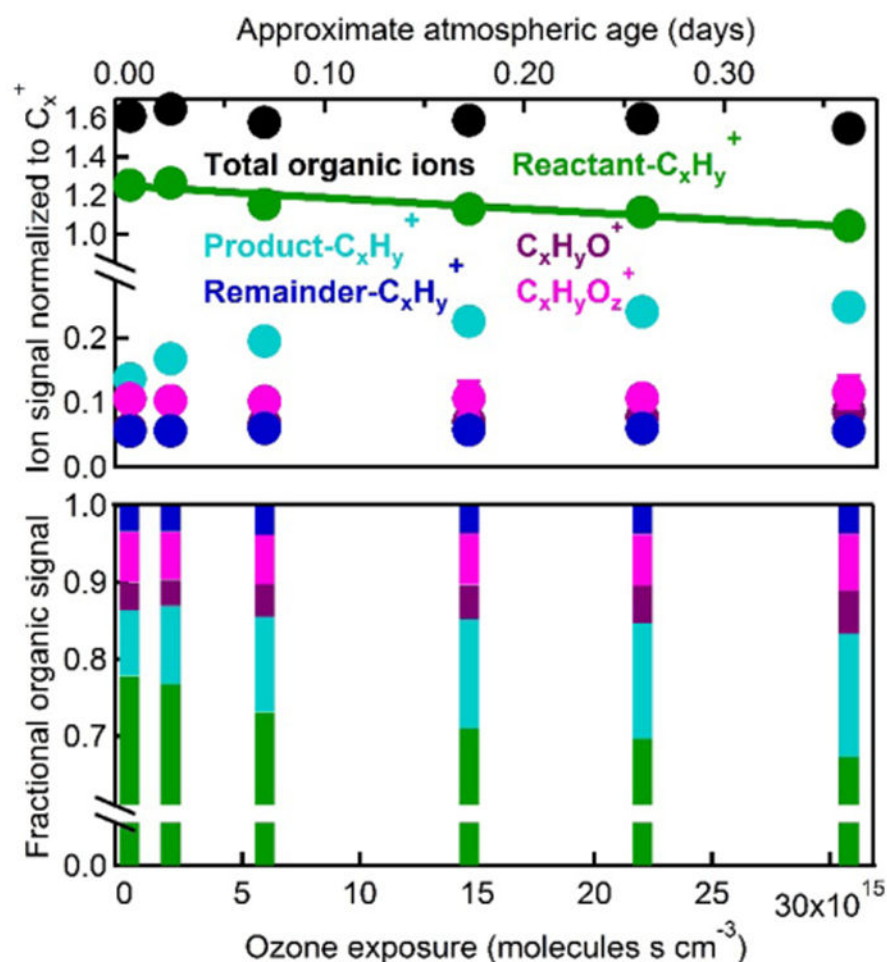
Figure 4.
Changes in ion signal for each class of ions as a function of ozone exposure. The approximate atmospheric age assumes a 24-h average ozone concentration of 40 ppbv. The $C_xH_y^+$ groupings are identical to those defined in the OH oxidation. Note the y-axis break in both panels. Top panel: the signals normalized to total C_x^+. The solid line shows the reactant $C_xH_y^+$ decay expected based on the second-order rate constant given in the text. As discussed in the text, the lowest ozone exposure is non-zero due to sonication altering the organic ion abundances. Bottom panel: fractional contribution of each ion class to the total organic signal.